Proceedings of ICFA Mini-Workshop on Tracking for Collimation in Particle Accelerators, CERN, Geneva, Switzerland, 30 October 2015, CERN Yellow Reports: Conference Proceedings, Vol. 2/2018, CERN-2018-011-CP (CERN, Geneva, 2018)

FLUKA-SIXTRACK Coupling for the SPS Scrapers

R.B. Appleby[1]*, F. Cerutti*[2] *and A. Mereghetti*[2*]
[1]UniMAN, Manchester, UK
[2]CERN, Geneva, Switzerland

Abstract

Recently, the FLUKA–SIXTRACK coupling has been set up to simulate with great detail the performance of cleaning systems in circular, ultra-relativistic accelerators. In a coupled simulation, the two codes run simultaneously while exchanging particle information; SIXTRACK tracks the beam through the accelerator lattice, whereas FLUKA simulates the interaction of the tracked beam with intercepting devices. Hence, the coupling combines the best of the two codes involved, characterised by a long history of development and benchmarking. The present work summarises the main outcomes of the first extensive application of the coupling to a study case – the SPS scrapers and their upgrade as proposed in the framework of the LIU project.

Keywords
SPS scrapers; collimation system; LIU SPS upgrade; Fluka-SixTrack coupling.

1 Introduction

The performance of collimation systems in circular accelerators can be predicted by numerical simulations capable of combining particle tracking through accelerator lattices and particle–matter interactions. In the last fifteen years, SIXTRACK [1–4] functionalities were extended and constantly updated with an engine for describing the main beam–matter interactions of relevance for simulating collimation systems of ultra–relativistic storage rings [5, 6]. In this way, it was possible to establish a solid simulation framework for designing and optimising cleaning systems, e.g. for the Large Hadron Collider (LHC) [7] and for the Relativistic Heavy Ion Collider (RHIC) [8]. Recent developments and applications are extensively reported in these proceedings, giving a complete overview of the ongoing work and key results achieved.

Recently a new simulation tool has been developed, combining the accuracy of SIXTRACK in tracking particles through accelerator lattices and the detailed scattering models of a full Monte Carlo code like FLUKA [9, 10]; this is the FLUKA–SIXTRACK coupling [11–14]. The present work gives an overview of the essential functionalities of the new tool (see Sec. 2), the technical aspects of which are described in more details in Ref. [11]. Afterwards, the first extensive application of the coupling is summarised; the studied case is the scraping system [15, 16] installed in the Super Proton Synchrotron (SPS), and its upgrade proposed in the framework of the LHC Injectors Upgrade (LIU) project [17, 18] (see Secs. 3 and 4). Finally, the robustness and maturity of the tool is probed with an extensive benchmark against measurements from a test of the scraper blades carried out with beam in 2013 (see Sec. 5).

*alessio.mereghetti@cern.ch.

https://doi.org/10.23732/CYRCP-2018-002.205.

2 The Coupling Between FLUKA and SIXTRACK

In a coupled simulation, FLUKA and SIXTRACK run simultaneously, and exchange particle information through a network port via a TCP/IP protocol managed by the FLUKAIO Application Programming Interface (API) [19].

The most relevant advantage of the FLUKA–SIXTRACK coupling is the deployment of two codes with a long history of development and bench–marking. The coupling allows to combine the refined physics models of particle–matter interactions of FLUKA with the accuracy of SIXTRACK in tracking particles through the accelerator lattice. In this way, multi–turn effects, relevant for collimation systems in circular machines, can be simulated with great detail and accuracy. For such systems, beam particles may need to go through the intercepting devices more than once before being definitively lost, either in the machine aperture or in the intercepting devices; hence, the dynamics by which particles are affected is a combination of single particle beam dynamics and interaction with matter. In addition, the shorter the effective length of the intercepting devices seen by beam particles, the larger the interplay between beam dynamics and physics of scattering. The flow of information is automatic, with the human intervention limited to the simulation set–up; moreover, the use of a network port for exchanging particle data avoids the use of files.

In a coupled simulation, transport through the accelerator lattice is regularly carried out by SIXTRACK until a portion flagged for transport in FLUKA is reached; at that point, beam particles are transferred to FLUKA, transported in its 3D geometry for simulating the interaction with the accelerator components of interest, and given back to SIXTRACK, to continue tracking. The user can flag as many FLUKA insertions as desired. The interfaces to FLUKAIO library on both the FLUKA and SIXTRACK side take care of the change of reference system and units of measurements between the two codes. The FLUKA–SIXTRACK coupling can be enabled with any form of tracking, i.e. in case of a thin or thick lens description of the accelerator, and in case of 4–dimensional or 6–dimensional tracking, including acceleration.

The original FLUKA and SIXTRACK codes have been extended by means of user routines and functions:

- An on–line aperture checking was implemented in SIXTRACK to stop tracking beam particles scattered out of beam–intercepting devices on trajectories not fitting into the mechanical aperture of the machine, avoiding to double count them at subsequent turns. This functionality is at the basis of the estimation of the distribution of losses along the ring, and it is crucial for the correct evaluation of the energy deposition in the beam–intercepting devices (and downstream elements). The check is performed during tracking ("on–line"), element by element and turn by turn;
- In order to take into account the varying distance between the beam and the scraper blades during their sweep (see Sec. 3), FLUKA user routines were coded to deal with moving bodies; similarly, dynamic kicks were implemented in SIXTRACK, to reproduce the change with time of the corrector strengths responsible for the magnetic bump foreseen by the LIU design (see Sec. 3). This implementation has been ported to the release version of SIXTRACK and extended in capability and flexibility [20].

3 The SPS Scrapers and their Upgrade

The SPS is equipped with scrapers, routinely used to ensure a clean injection into the LHC. They are installed in the Long Straight Section 1 (LSS1) of the SPS, which also hosts the beam dumping system[1]. The scrapers are composed by movable graphite blades, 1 cm in length (see Fig. 1, left frame); one per plane, they are swept through the beam to remove tails at the desired transverse position. Scraping is performed at the end of the ramp, immediately before beam transfer to the LHC, in order to minimise

[1] As it will seen later (see Sec. 5.1), this fact has consequences on loss measurements in the region.

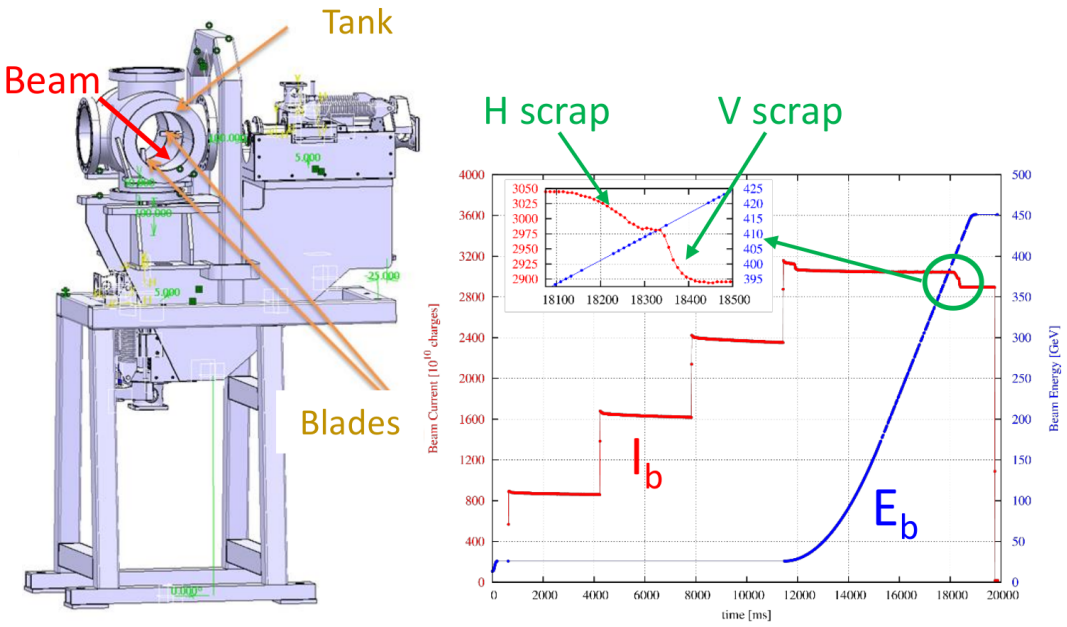

Fig. 1: Left frame: 3D view of the scraper assembly. Right frame: typical patterns of beam current and energy during an SPS cycle. The zoom shows the tiny intensity decrease due to tail scraping on both the horizontal and the vertical plane as done during regular operation.

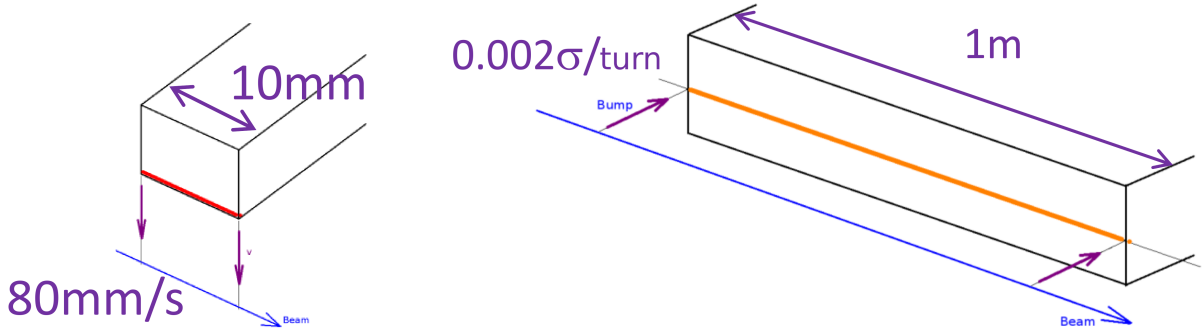

Fig. 2: Schematics of the present mechanical scrapers (left frame) and those proposed as upgrade (right frame). The sketch shows the beam trajectory, the relative beam–absorber movement with its speed, and essential dimensions of the devices.

tail re–population. Hence, they are kept off the beam for most of the SPS cycle and only at its end they perform the necessary cleaning action (see Fig. 1, right frame). As such, they are fast betatron scraping devices.

In the context of the LIU project, it was proposed to study a possible upgrade of the SPS scraping system from a thin blade mechanically swept through the beam to a bulk absorber block against which the beam is steered by means of a magnetic bump (see Fig. 2). The study was triggered not to overcome a specific limitation of the present system, but as a possible alternative to improve flexibility and limit secondary radiation escaping the beam–intercepting device, and hence induced radioactivity. In fact, though being more complex than the present one, the new design would overcome some limitations intrinsic in the design of the system presently in operation:

Table 1: Beam parameters used in simulation: normalised emittance (ϵ_{N}), standard deviation of the momentum distribution (σ_δ), bunch population ($\mathrm{N_b}$), total beam intensity ($\mathrm{N_p}$), total stored energy ($\mathrm{E_T}$), number of bunches ($\mathrm{n_b}$), and beam energy (E_{b}).

Scraper Design	ϵ_{N} [μm]	σ_δ [10^{-4}]	$\mathbf{N_b}$ [10^{11}]	$\mathbf{N_p}$ [10^{13}]	$\mathbf{E_T}$ [MJ]	$\mathbf{n_b}$ []	$\mathbf{E_b}$ [GeV]
Present	1	1	1.15	3.31	2.38	288	450
LIU	2.5	5.25	2.5	7.2	5.52		

1. it would allow to better control the beam–impact conditions at the absorber;
2. it would imply no mechanical movements, with consequent no mechanical wear of components.
3. it would make cleaning more efficient, since a longer absorber increases the probability for a proton to undergo a nuclear inelastic interaction at the first encounter, and hence being ultimately absorbed by the system;
4. it would allow to have softer spectra of particles escaping the absorber.

The first two bullets come from the choice of deploying a magnetic bump, whereas the other two come from the use of a long absorber block. As for the present scrapers, the new system would be triggered at the end of the SPS cycle, raising the bump until scraping is accomplished. The new system would be installed in the SPS LSS6.

4 Comparison of Systems

In order to characterise the two systems, a large simulation campaign was carried out [12]. Numerical simulations were performed with the FLUKA–SIXTRACK coupling (see Sec. 2), set up on purpose for these studies. The relevant observables are the density of energy deposition in the material interacting with the beam (see Sec. 4.1), the evolution with time of the beam current during scraping (see Sec. 4.2), and the distribution of losses along the ring (see Sec. 4.3). Results refer to the case of 0 σ scraping, i.e. when the whole beam is scraped away (including the core) with the blade swept at the beam closed orbit. This is taken as design case, even if it is an extreme one, since it maximises the energy deposition per beam proton [12] even though it is neither an operational case, as the scrapers are meant to scrape away tails, nor an accidental scenario. Hence, the simulated case represent a potential accident scenario, where by operational mistake the full beam is totally scraped at full intensity. Scraping on the horizontal plane is considered.

Simulations consider full beam intensity (i.e. 288 bunches), with Gaussian transverse and momentum distributions. The considered beam parameters are reported in Table 1. It should be noted that, while the number of bunches always remains 288 per injection into the LHC, the highest bunch population at SPS extraction considered for the LIU design is more than twice the one of nominal LHC beams available in the SPS at the time of the study [18].

4.1 Energy Deposition

Figure 3 shows a 3D view of the energy deposition maps superimposed to the geometry of the scraper blade and of the LIU scraper absorber. The distribution of the energy deposition is collapsed on the very first layers of material directly impacted by the beam on the plane of movement; on the other plane, the distribution keeps memory of the original beam size, implying a dependence on machine optics and beam parameters.

Table 2 reports the maximum values of expected energy deposition. Values per impacting proton for the LIU system are more than a factor 3 lower than those for the present system, mainly because of the different designs [12]. The values in kJ/cm^3 are obtained from those in GeV/cm^3 taking into

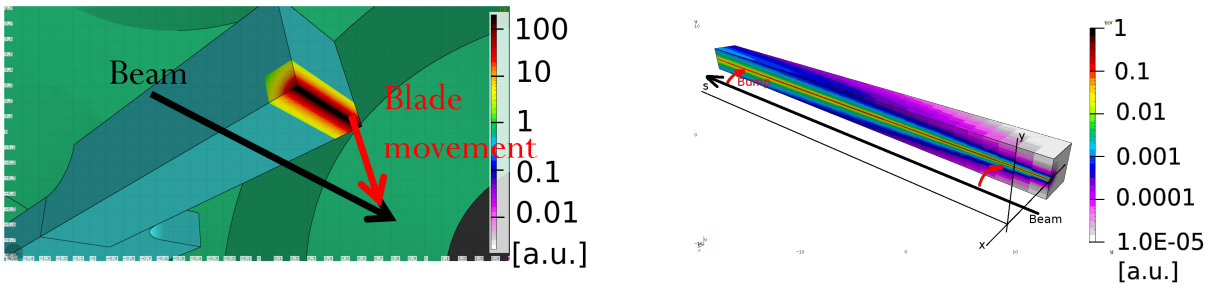

Fig. 3: 3D view of the energy deposition maps superimposed to the geometry of the scraper blade (left frame) and of the LIU scraper absorber (right frame) proposed as upgrade. The views have been produced with FLAIR [21]. The relative movement between the beam closed orbit and the absorbing devices is also shown.

Table 2: Peak energy deposition in the absorbing material of the scrapers in case of 0 σ scraping at full beam intensity. Values are given per impacting proton (second column) and per per bunch train and the respective bunch populations (Tab. 1).

Scraper Design	$\mathbf{E}_{\mathrm{max}}$ [GeV/cm^3]	[kJ/cm^3]
Present	30–35	160–185
LIU	10–11	115–130

account 288 bunches and the respective bunch populations, reported in Tab. 1; hence, the factor 3 of difference is decreased to 40 %. The absolute numbers should be compared with the reference value of 12.8 kJ/cm^3, equivalent to the energy density necessary to locally reach the sublimation temperature of graphite of 3600°C[2]. The values of maximum energy deposition show the severity of the simulated scenarios, implying a local damage of the absorbing material. The maximum value found for the LIU scraper increases by 50 % when the normalised emittance is decreased to 1 μm.

4.2 Evolution of Beam Intensity with Time

Figure 4 shows the time profile of the beam intensity during scraping at 0 σ for the two systems. The profile of the present system is dominated by the beam dimensions and the blade speed for a substantial fraction of time; once the blade reaches the centre of the beam, an exponential attenuation is seen and the material density and the blade thickness become the key parameters. In fact, with an inelastic interaction length of 45 cm in graphite at SPS top energy (i.e. 450 GeV, see Tab. 1), a beam proton requires on average 45 turns before undergoing an inelastic event and being hence absorbed.

The profile of the upgraded system shows a linear dependence on the speed with which the magnetic bump is raised. This is expected, because with a 1 m–long graphite absorber, a proton at SPS flat top energy (i.e. 450 GeV, see Tab. 1) has a high chance to undergo a nuclear inelastic event with a single passage through the absorber.

As a matter of fact, with the present operational parameters of the two systems (see Fig. 2), there is no difference on the time required to fully accomplish scraping, as the beam is reduced to a few % in ∼1000–1500 turns for both systems. For the present system, this time scale is the result of a combination of two factors: on the one hand, the time required by the blade to reach the centre of the beam (i.e. to have all beam protons at reach) determined by the speed of the blade; on the other hand, the average time

[2]This value was calculated simply integrating the specific heat as a function of temperature.

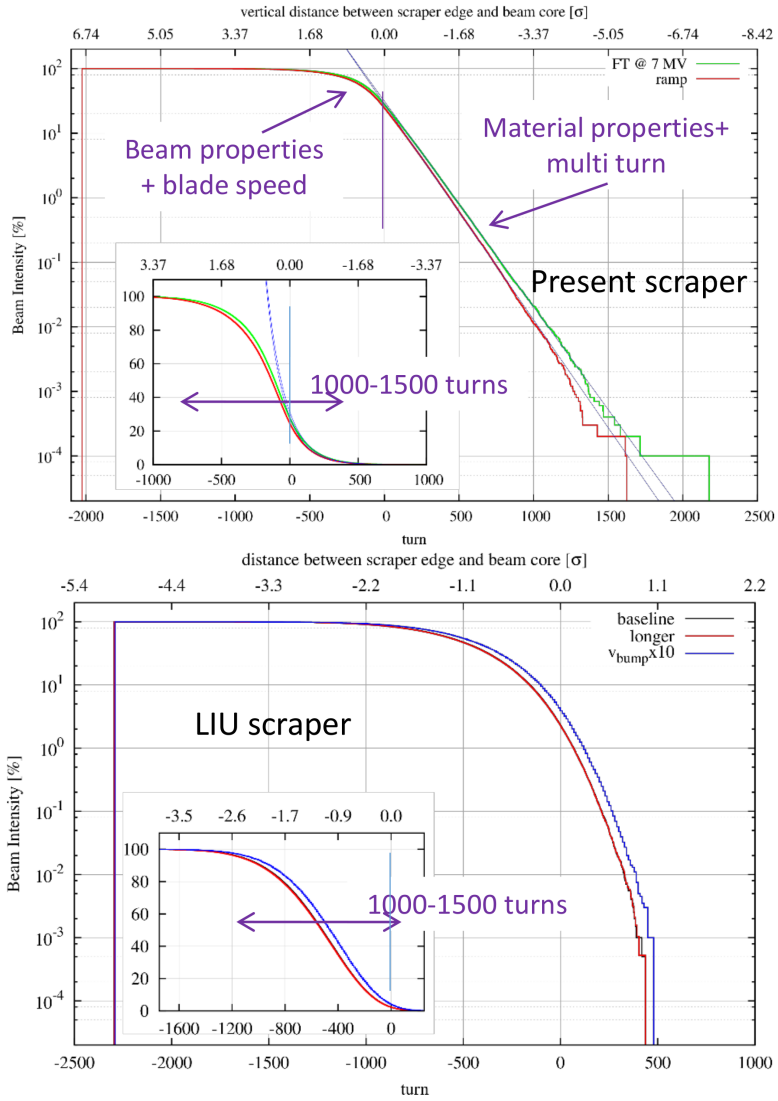

Fig. 4: Time profile of the beam current during scraping in case of the present scraping system (upper frame) and in case of the LIU design (lower frame) for 0 σ scraping. The origin of the horizontal axes marks the moment when the cutting edge of the absorber reaches the position of the closed orbit. The green curve in the upper frame refers to simulations run at flat top energy with the nominal 7 MV RF voltage, whereas the red curve was obtained simulating the ramp, at around 400 GeV. The black curve in the lower frame refers to the baseline upgraded system (see Sec. 3), whereas the red curve has been obtained with the absorber twice in length. The blue curve in the same frame refers to the case with the magnetic bump 10 times faster; for the sake of clarity, the horizontal scale has been expanded by the same factor.

necessary to a proton to undergo a scattering event leading to its loss. For the upgraded system, the time scale is given by the speed with which the bump is raised.

The upper frame of Fig. 4 also shows the case of scraping towards the end of the ramp, as it happens in reality; the curve was obtained taking into account acceleration in SIXTRACK. Scraping starts earlier, due to the slightly larger spot size at lower beam energy; moreover, the exponential part is slightly steeper, in accordance to a slightly larger beam emittance, implying trajectories closer to the machine aperture and larger impact angles (and hence longer paths in the blade), and to larger scattering angles. The lower frame also shows that a longer absorber for the LIU design does not reduce the time

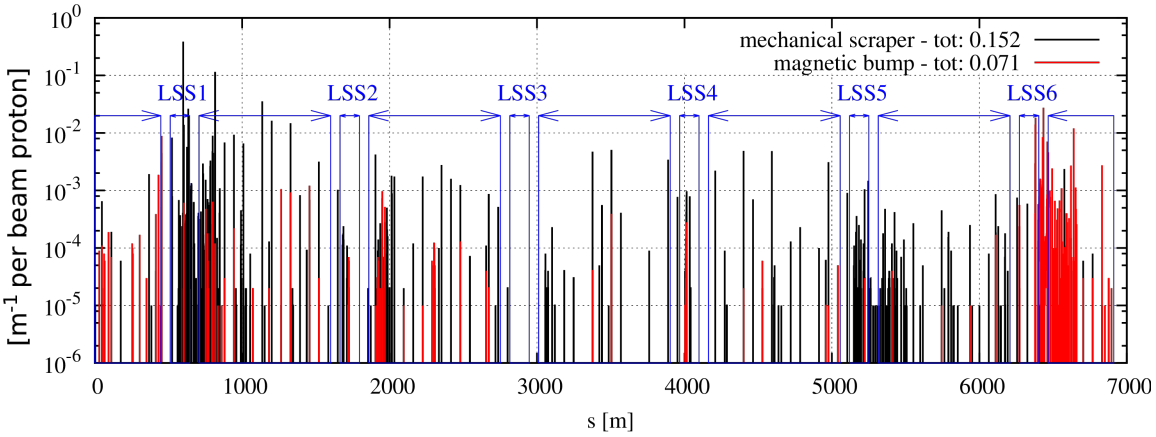

Fig. 5: Distribution of losses along the SPS ring during scraping for the two systems; only protons lost with $\delta < 2$ % are shown. The key in the plot reports the fraction of protons lost in the ring.

for scraping.

4.3 Loss Distribution

Figure 5 shows the distribution of losses along the SPS ring during scraping for the two systems; the shown distribution takes into account only lost protons with $\delta < 2$ %. Losses concentrate in the cells immediately downstream of the scraping devices, including the first cells of the downstream arcs. Local peaks are also found further into the arcs. As a matter of fact, the LIU design decreases the overall losses by a factor 2.

5 The Robustness Test and the Benchmark of Simulation Results

The very harsh conditions of energy deposition predicted by simulations (see Sec. 4) triggered the request of a test with beam where these conditions could be reproduced and values verified (see Sec. 5.1). After the test, the blades were dismounted for detecting possible damage.

The test was also the occasion for an extensive benchmark of the simulation tool (see Sec. 5.2); the main observables are the time evolution of the beam current as recorded by the Beam Current Transformer (BCT) and the loss pattern measured by the Beam Loss Monitors (BLMs) during set up of the test.

5.1 The Robustness Test

The test took place on 16$^{\text{th}}$ February 2013, at the end of the SPS activity during the LHC Run I. To probe their endurance, the blades were probed with scraping the whole beam (i.e. 0 σ scraping) at full intensity (see Tab. 1, "present" scraper design), since this is the scenario for which the peak energy deposition predicted by simulation is the highest (see Sec. 4). The test was performed at 450 GeV, with a total beam intensity of 3.1 10^{10} charges. The spare scrapers were used in order to more easily disentangle the damage due to the test from possible damage due to regular operation. Both planes were probed independently, one after the other one.

At the very moment of the test, extremely high vacuum spikes were recorded at the vacuum gauges immediately upstream of the scrapers; the spikes were three orders of magnitude larger than the regular values with circulating beam. Such a vacuum deterioration is sign of material emission by the scraper blades. Optical scans of the surface of the blades [22] revealed an increase in the porosity of the material, from a value of $\sim$10 % far from the blade edge up to $\sim$30 % in the region nearby the edge.

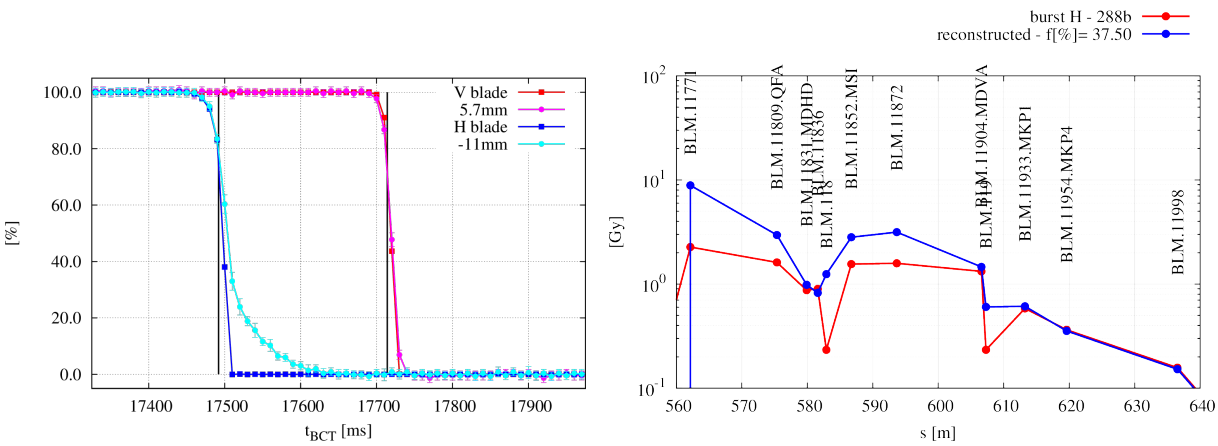

Fig. 6: Left frame: time profile of the normalised BCT signal for full beam scraping during the test of each blade (red and blue curves) and in case of scraping at the same transverse position with low–intensity beams (magenta and cyan curves). The vertical black lines mark the timing of the dump as from logging. Right frame: BLM pattern recorded during the robustness test of the horizontal blade (red curve) and the one reconstructed with Eq. 1 (with signals from pure scraping and pure dumping events, blue curve), which matches the last three BLMs in LSS1. The fraction reported in the legend of the blue curve reports the amount of scraped beam necessary for the matching.

Further analyses [12] showed that the beam was prematurely dumped while testing the blades by the BLM at the scraper. Secondary particle showers generated by proton inelastic interactions in the blades were so intense that the dump threshold was reached before scraping was completed. In fact, the time profiles of the normalised BCT signal while scraping during the tests are different from those taken with low–intensity beams and the same scraping settings (see Fig. 6, left frame); the difference is clearly visible for the horizontal blade, whereas for the vertical blade the difference is less evident, though still present.

The same conclusion can be drawn from the signals of the LSS1 BLMs (see Fig. 6, right frame). In fact, the patterns from a pure dump event and a pure scraping event can be linearly combined to reconstruct the pattern measured during the tests. The linear combination can be written as

$$R_{\mathrm{i,test}} = sR_{\mathrm{i,scrp}} + (1-s)R_{\mathrm{i,dump}}, \tag{1}$$

where R_{i} represents the signal from the i–th BLM, s is the amount of scraped beam, and the subscripts "test", "scrp" and "dump" refer to the signals recorded during the test, a pure scraping event and a pure dump event, respectively. The linear combination is necessary since the values logged by the SPS BLMs electronics are integrated over the entire SPS cycle; hence, in case of partial scraping, the BLM pattern in LSS1 reflects not only the action of scraping, but also the action of dumping the circulating beam, since LSS1 hosts also the beam dumping system (see Sec. 3). Moreover, the electronics of most of the LSS1 BLMs were at saturation during the test; therefore, the proper matching between the recorded pattern and the one reconstructed via Eq. 1 is established only for those BLMs surely out of saturation, i.e. the last three in LSS1.

A premature dump implies a load on the blades lower than the one predicted by simulations. Table 3 reports the amount of beam scraped during the robustness test of each blade as estimated with BCT measurements and BLM measurements. In the case of the former set of measurements, the amount of scraped beam corresponds to the value of the normalised BCT profile with low–intensity beams at the time of dump; for the latter set of measurements, the amount of scraped beam is found when the readouts of the last three BLMs in LSS1 are matched by the profile reconstructed with Eq. 1. The two methods give quite different estimations; while the estimation via the BCT is affected by the limited BCT

Table 3: Amount of beam scraped during the robustness test of each blade as estimated via BCT measurements and BLM measurements (see Fig. 6). The consequent energy density in the most loaded point of the blade is reported as well.

Tested	BCT–based		BLM–based	
Blade	[%]	[kJ/cm^3]	[%]	[kJ/cm^3]
H	∼20	20–24	38	37–46
V	∼30	27–37	44	38–53

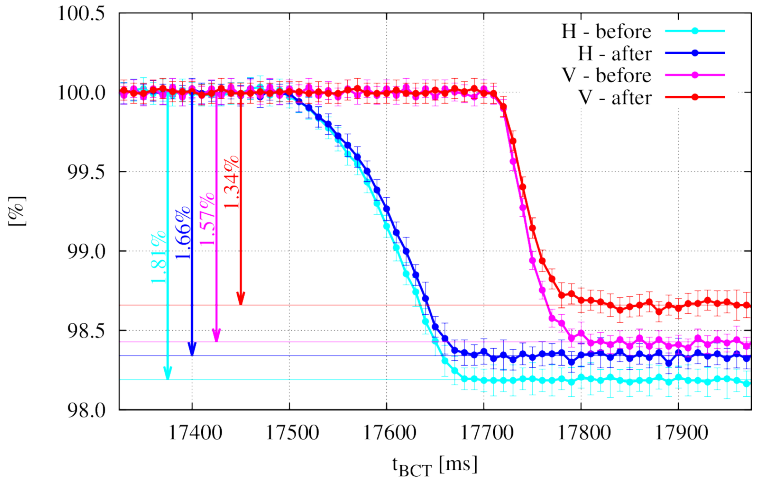

Fig. 7: Time profiles of the normalised BCT signal for regular scraping before and after the robustness test.

bandwidth (3 dB at 50 Hz) and the poor sampling rate (10 Hz) with respect to the timing of scraping, the one via the BLMs seems to be more reliable, since it is not affected by any timing issue and it is based on integral quantities measured by not saturated monitors. It can be concluded that not even half of the beam was scraped away before dumping. The energy density in the most loaded point of the blade is reported as well in Tab. 3. Even in the case of the earliest dump (i.e. for the horizontal blade), values are much larger than the heat required to locally sublimate graphite, in accordance with the vacuum spikes registered during the tests and the aforementioned crystallographic analyses.

The cleaning performance of the blades for regular scraping was checked to spot any loss of performance following the induced damage. Therefore, the time profiles of the normalised BCT signal for regular scraping before and after the robustness test were compared (see Fig. 7); very minor differences were found, most probably due to a change in beam profile or emittance, or a drift in the closed orbit [12].

5.2 The Benchmark of Simulation Results

The robustness test was also taken as occasion for an extensive benchmark of the simulation tool. BCT readouts and BLM measurements during the set up of the test were used, recorded when scraping with each tested blade at different transverse positions. Measurements were taken with low–intensity beams in order not to deal with saturated BLM readouts.

The benchmark against the normalised BCT signals allowed to reconstruct the actual speed and angle of the blades during the tests; in fact, these parameters affect the time profile of the beam current during scraping (see Fig. 8). Different values were tested in simulation, until a reasonable matching of the profiles with all scraping settings was found. Table 4 summarises the range of values used in

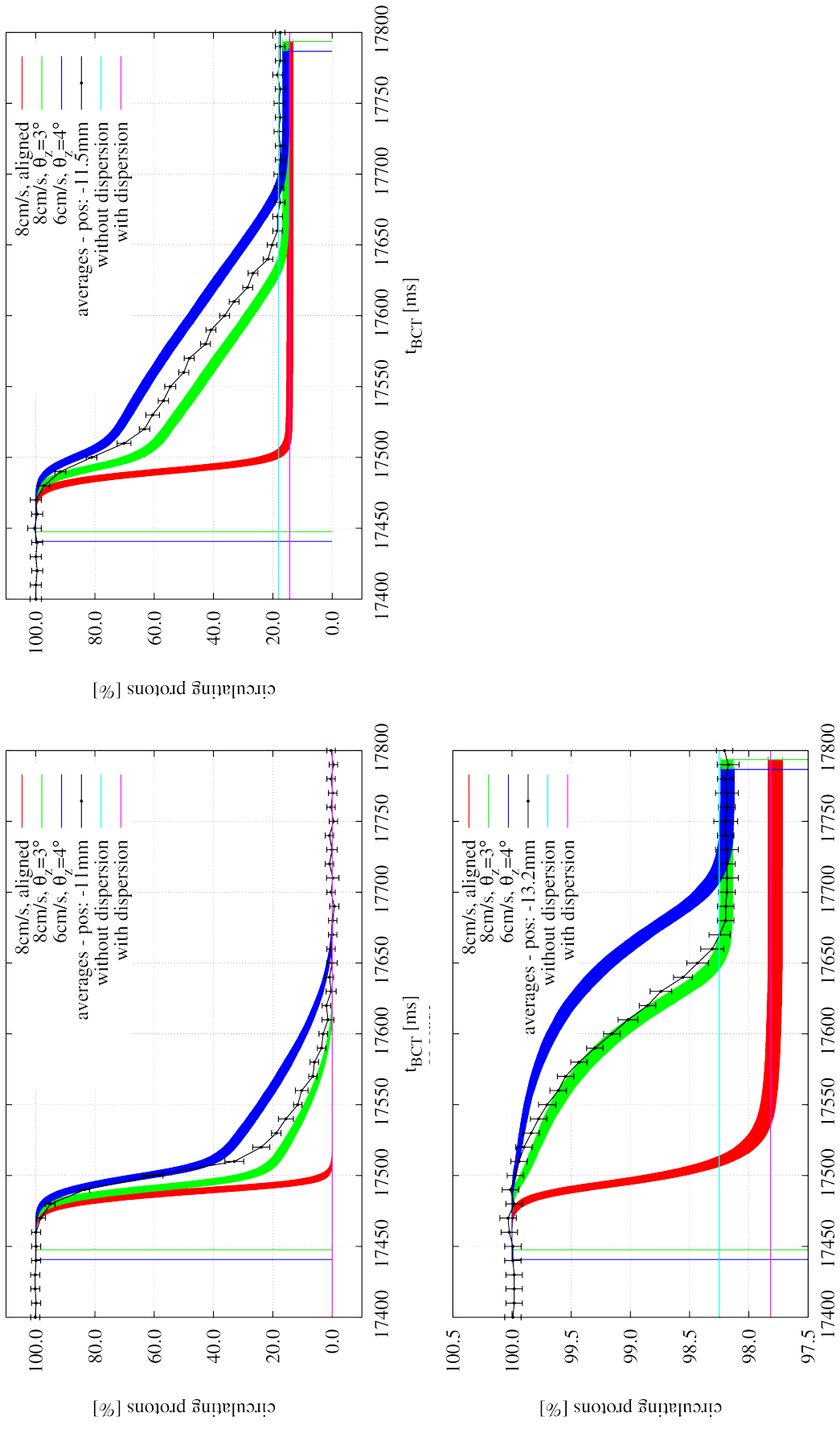

Fig. 8: Time profiles of the normalised beam intensity measured by the BCT (black points) and as predicted by simulation for full beam scraping (0 σ scraping, upper–left frame) intermediate scraping (i.e. at 500 μm from the beam centre, upper–right frame) and regular scraping (i.e. at 2.2 mm, lower–left frame). The case of the horizontal blade is shown, whereas the one of the vertical blade can be found in Ref. [12]. In each frame, the black curves show averages over consecutive fills with the same beam intensity and scraping settings, and the error bars show the 1 σ dispersion of data. Three combinations of blade speed and tilt are shown, and the error bars show the statistical error only. The magenta and cyan lines show the beam intensity after scraping predicted analytically in case dispersion effects are and are not taken into account, respectively.

Table 4: Speed and angle of the tested scraper blades as reconstructed with the benchmark against normalised BCT profiles (see Fig. 8). The nominal values are reported as well.

	Speed [cm/s]	**Angle** [°]
H	6–8	3–4
V	<6	<0.5
nominal	8	0

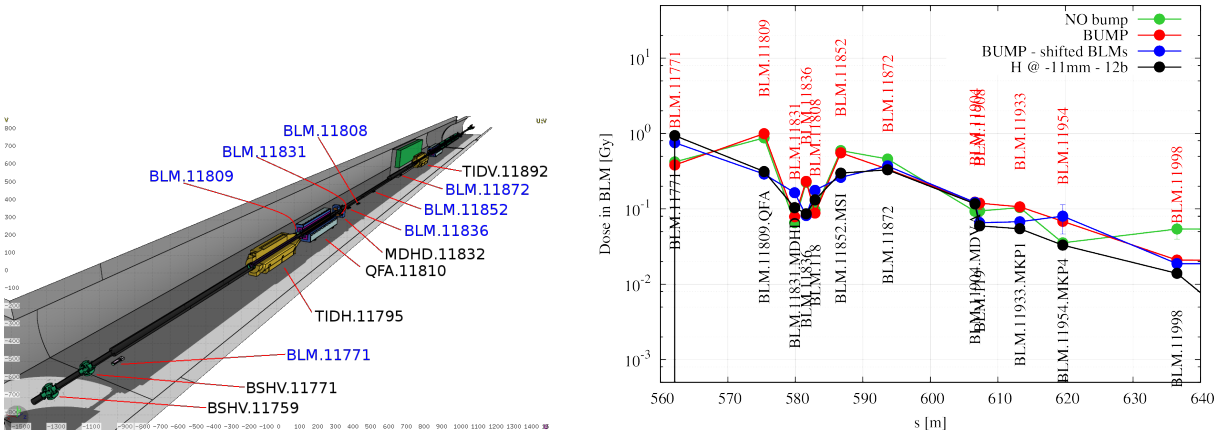

Fig. 9: Left frame: 3D view of the FLUKA model of the SPS LSS1, downstream of the scrapers. The view was generated with FLAIR [21]. Right frame: BLM signals as measured during full beam scraping at low intensity (black line) and as reproduced by simulations in case the permanent magnetic bump in the SPS LSS1 is taken into account (red curve) or not (green curve). Simulation results with transverse offsets applied to BLMs are shown as well (blue curve).

simulation giving the best matching to measurements, along with the nominal values.

The benchmark against BLM readouts required to describe in FLUKA the SPS LSS1 downstream of the scrapers (see Fig. 9, left frame). In fact, the readouts reflect the development of secondary particle cascades, started by inelastic events taking place in the scraper blades or by beam protons hitting the machine aperture. Therefore, details regarding geometry and materials of the elements nearby the monitors reached by the cascades are relevant for the purpose of the bench–marking. As it can be seen (see Fig. 9, right frame), simulation results dramatically depend on the transverse position of the BLMs. Because of the non–perfect agreement between technical drawings, the BLMs were simulated also with transverse offsets from their nominal positions, in order to give a hint of the sensitivity (red vs blue curves in the same figure). Moreover, the effect of a permanent magnetic bump[3] on BLM readouts has been addressed as well (red vs green curves in the same figure).

6 Conclusions

The FLUKA–SIXTRACK coupling allows to simulate with great detail the performance of cleaning systems in circular machines in a large variety of applications. This is possible thanks to the accuracy of the two codes involved, characterised by a long history of development and bench–marking. The present work has summarised the main outcomes of the first extensive application of the coupling to a study case,

[3] A permanent magnetic bump is present in the SPS LSS1 to ease dumping. The bump is achieved offsetting three consecutive main quadrupoles.

i.e. the SPS scrapers and their upgrade as proposed in the framework of the LIU project.

The two systems were compared in terms of energy deposition in the absorbing medium, evolution of beam intensity with time during scraping, and losses induced around the ring. The focus was in particular on the case of scraping at 0 σ, as this scenario is characterised by the highest density of energy deposition in the absorbing material. Despite its complexity, the upgraded system is characterised by lower loads on the absorbing material and lower losses around the ring; moreover, thanks to its conceptual design, it intrinsically offers more control on the impact conditions of the beam on the absorber during scraping.

A robustness test of the system presently installed was carried out at the end of the SPS activity in 2013, to verify damage levels in the blades. The test also gave the opportunity for an extended benchmark of the simulation tool against BCT readouts during scraping and BLM signals downstream of the scrapers. The positive outcomes of the benchmark indicate the maturity and accuracy of the simulation tool.

Acknowledgements

We wish to thank K. Cornelis, O. Mete, V. Kain and the SPS operation team for setting up and conducting the robustness test.

References

[1] F. Schmidt, SIXTRACK Version 4.2.16: Single Particle Tracking Code Treating Transverse Motion with Synchrotron Oscillations in a Symplectic Manner; User's Reference Manual, CERN–SL–94–56(–AP), CERN, Geneva, Switzerland (1994).

[2] G. Ripken and F. Schmidt, A Symplectic Six–Dimensional Thin–Lens Formalism for Tracking, CERN–SL–95–12(–AP), DESY–95–063, CERN, Geneva, Switzerland (1995).

[3] SIXTRACK website: `http://sixtrack.web.cern.ch/SixTrack`.

[4] R. De Maria *et al.*, these proceedings.

[5] G. Robert–Demolaize, R.W. Assmann, S. Redaelli, F. Schmidt, Proc. Particle Accelerator Conf. (PAC'05), Knoxville, TN, USA, 2005, paper FPAT081, pp. 4084–4087.

[6] R. Bruce *et al.*, these proceedings.

[7] R.W. Assmann *et al.*, in Proc. 10$^{\text{th}}$ European Particle Accelerator Conf. (EPAC'06), Edinburgh, Scotland, UK, Jun 2006, paper TUODFI01, pp. 986–988.

[8] G. Robert–Demolaize and A. Drees, these proceedings.

[9] T.T. Bohlen *et al.*, The FLUKA Code: Developments and Challenges for High Energy and Medical Applications, Nuclear Data Sheets 120, 211–214 (2014)

[10] A. Ferrari *et al.*, FLUKA: a multi–particle transport code, CERN–2005–10 (2005), INFN/TC_05/11, SLAC–R–773.

[11] V. Vlachoudis *et al.*, these proceedings.

[12] A. Mereghetti, Performance Evaluation of the SPS Scraping System in View of the High Luminosity LHC, Ph. D. thesis, UniMAN, Manchester, UK (2015).

[13] `Twiki` of the FLUKA–SIXTRACK coupling: `https://twiki.cern.ch/twiki/bin/view/FlukaTeam/CouplingSVNRepositories`.

[14] `SVN` repository of the FLUKA–SIXTRACK coupling code (CERN credentials required): `http://svn.cern.ch/reps/fluka_coupling`.

[15] H. Burkhardt and R. Schmidt, Intensity and Luminosity after Beam Scraping, CERN–AB–2004–032–ABP (2004).

[16] G. Arduini and H. Burkhardt, Transverse Tail Scraping in the SPS for Clean LHC Injection, EDMS doc. 772782 (2006).

[17] LIU website: `espace.cern.ch/liu-project`.

[18] J. Coupard *et al.* (Eds.), LHC Injectors Upgrade – Technical Design Report – Volume I: Protons, CERN–ACC–2014–0337 (2014).

[19] `Twiki` of the FLUKAIO protocol: `twiki.cern.ch/twiki/bin/view/FlukaTeam/FlukaIO`

[20] K. Sjobaek, these proceedings.

[21] V. Vlachoudis, in Proceedings of the Conf. on Mathematics, Computational Methods & Reactor Physics (M&C 2009), Saratoga Springs, New York (2009).

[22] F. Léaux, Microscopic Observations of Irradiated Graphite Scraper Blades, EDMS. 1339153, CERN, Geneva, Switzerland (2014).